Boundary Value Problems
a SpringerOpen Journal

CrossMark

Peristaltic motion of MHD nanofluid in an asymmetric micro-channel with Joule heating, wall flexibility and different zeta potential

S. Noreen[1], S. Waheed[1] and A. Hussanan[2,3*] (iD)

*Correspondence:
abidhussanan@tdtu.edu.vn
[2]Division of Computational
Mathematics and Engineering,
Institute for Computational Science,
Ton Duc Thang University, Ho Chi
Minh City, Vietnam
[3]Faculty of Mathematics and
Statistics, Ton Duc Thang University,
Ho Chi Minh City, Vietnam
Full list of author information is
available at the end of the article

Abstract

A mathematical scrutiny is introduced for the flow of magneto-hydrodynamic nanofluid through an asymmetric microfluidic channel under an applied axial electric field. The impacts of wall flexibility, Joule heating and upper/lower wall zeta potentials are considered. Electric potential expressions can be modeled in terms of an ionic Nernst–Planck equation, Poisson–Boltzmann equation and Debye length approximation. Appropriate boundary conditions have been utilized to get the results of highly nonlinear coupled PDEs numerically. The impact of physical factors on the characteristics of flow, pumping, trapping and heat transfer has been pointed out. The outcomes may well assist in designing the organ-on-a-chip like gadgets.

MSC: 76W05; 76E25; 35Q35

Keywords: Peristalsis; Electro-osmosis; Magneto-hydrodynamic (MHD) nanofluid; Trapping

1 Introduction

Current past reveals that the extra consideration has been given to area of research entitled "microfluidics" so that advances in microfabrication technologies are accessible. In a microfluidic system, electroosmotic flow (EOF) is significant. Electroosmosis is basically an electrokinetic mechanism, in which we examine the ionic development of fluids affected by electric fields. Due to this process, a Stern layer (a charged surface with a high concentration of counter ions) is created. Resulting Stern layer with diffusing layer forms an Electric Double Layer (EDL). The potential (interfacial) between diffuse double layer and Stern layer is called zeta potential, a prominent aspect of many electrokinetic mechanisms. Electrokinetic transportation has become a vivid area of modern fluid mechanics. The combined impacts of electrokinetic and peristaltic phenomena are critical in controlling biological transport mechanisms. Electrokinetics contains electrophoresis, electroosmosis, diffusiophoresis and several other phenomena. Many microfluidic apparatus such as Lung chips, proteomic chips, lab-on-a-chip (LOC), portable blood analyzers, micro-peristaltic pumps, organ-on-a-chip, micro-electro-mechanical systems (MEMS), micro-peristaltic pumps, DNA and bioMEMS, as well as microscopic

full analysis systems are built upon the ideology of EDL and electroosmosis. Moreover, microfluidic apparatus is also associated with MEMS, automation and parallelization, cost-effectiveness analysis, integration, miniaturization, separation, study of biological/chemical factors and high efficiency progression. Bandopadhyay et al. [1] examined the peristaltic modulation of electroosmotic flow in the microfluidic channel for the viscous fluid. Shit et al. [2] analyzed the rotation of EOF in a non-uniform micro-fluidic channel through slip velocity. Tripathi et al. [3] discussed the impacts of electroosmosis and peristalsis, for unsteady viscous flow. Ranjit et al. [4] worked on the electromagneto-hydrodynamic flow via peristaltically induced microchannel along the effects of Joule heating and wall slip. Furthermore, Tripathi et al. [5] scrutinized the mathematical model on electroosmosis in peristaltic biorheological flow through an asymmetric microfluidic channel. Jhorar et al. [6] proposed the peristaltic modulation of electroosmosis in an asymmetric microfluidic channel for viscous fluid. Ranjit et al. [7] explained the effect of zeta potential and Joule heating through porous microvessel on peristaltic blood flow. In addition, Prakash et al. [8] investigated the EOF Williamson ionic nano-liquids in a tapered microfluidic channel under the effects of peristalsis and thermal radiation. Tripathi et al. [9] considered the electroosmosis of microvascular blood flow.

In the existing literature, traditional liquids such as water and natural oil fail to accomplish the current demands for improving thermal conductivities. Currently, nanofluid research is a major topic of research because it enhances the thermal conductivity of conventional liquids. Nanofluidic flow problem has numerous uses in biomedical engineering such as the delivery of a drug by using nanoparticles, heat exchanges and tumor cure. However, researchers have paid great attention to the all above-mentioned phenomenon. Das et al. [10] found that the effect of electrical and thermal conductivities of the wall in a vertical channel for nanofluid flow. Hassan et al. [11] explored the properties of the wall in a porous channel, for the peristaltic flow of MHD nanofluid. Alghamdi et al. [12] demonstrated the smooth solutions for three-dimensional Hall-MHD equations through regularity criteria. Ahmed et al. [13] discussed the generalized time-convection of non-local nanofluids in a vertical channel. Pramuanjaroenkij et al. [14] studied the enhancement of heat transfer for the hybrid thermal conductivity model of nanofluid, numerically. Moreover, Arabpour et al. [15] analyzed the influence of slip boundary conditions on the flow of double-layer microchannel nanofluid. Akbarzadeh et al. [16] investigated the first two laws of thermodynamics for nanofluid flow with porous inserts and corrugated walls in a heat exchanger tube. In addition, Mosayebidorcheh et al. [17, 18] explained the peristaltic flow of nanofluid and heat transfer through asymmetric straight and divergent wall channels. Rahman [19] assumed the expansion/contraction of MHD nanofluid through permeable walls. Prakash et al. [20] demonstrated the effect of thermal radiation on electroosmosis modulation and peristaltic transport of ionic nano-liquid in biological microfluidic channel.

Peristaltic flow is a flow by wave propagation along the flexible walls of channel. Peristalsis is an inbuilt feature of many biomedical and biological systems. Physiologically, it plays a crucial role in several situations, for example, function of ureter, mixing of food and chyme transport in the tract of gastro-intestine, transportation of oocytes in the fallopian tube of females and the transmission of sperms in the male reproductive tract. Moreover, it is also useful in transport of cilia and bile duct, movement of lymph in lym-

phatic vessels and vascular movement of blood vessels, roller pump design (for pumping fluids without contact of pumping machinery) in peristaltic and acupressure pumps for cardiopulmonary and dialysis machinery. The updated version of hose pumps are operated by the peristaltic principle. Peristalsis is particularly advantageous for the transportation of slurries and chemicals that are corrosive in nature; therefore, preventing the rotation of pump drive and damage to moving parts. On a LOC device, it is generally essential to deliver a small amount of biological fluid by peristalsis (in a smaller level) than in a typical LOC system. Thus, contamination of the sample is prevented. Such uses have unlocked a new approach for doctors and mathematicians to maneuver their gadgets to scrutinize better results. Gala et al. [21] explained the regularity criterion for Boussinesq equations with respect to zero thermal conductivity. Also, Gala et al. [22] described the weak solutions for quasi-geostrophic equations through uniqueness criteria in Orlicz–Morrey spaces. Nanofluid transport in an asymmetric peristaltic flow was incorporated by Noreen [23]. Latha et al. [24] used the impacts of heat dissipation on the Jeffery and Newtonian fluid of peristaltic flow in an asymmetric channel. Besides, Latha et al. [25] also worked on the asymmetric channel with partial slip conditions for peristaltic transport of couple stress fluid. Noreen [26] determined the magneto-thermal hydrodynamic peristaltic transport for Eyring–Powell nanofluids through an asymmetric conduit. Furthermore, Abd Elmaboud et al. [27] developed the peristaltic transport for couple stress fluid through the rotating channel. Bhatti et al. [28] developed the peristaltic impulsion of solid (magnetic) particles in biological fluids, thermally. The electromagnetic transport for two-layer immiscible liquids incorporated in [29] by Elmaboud et al. Moreover, Saravana et al. [30] depicted the effect of heat transfer and flexible walls on the peristaltic flow of a Rabinowitsch fluid through an inclined channel.

The literature review showed that most of earlier studies dealt with electrokinetic or peristaltic pumping to drive fluid flow. The combined outcomes of peristalsis and electrokinetic phenomena can be critical for improving/controlling the mechanism of peristaltic transport. Inspired by the extensive uses of electroosmosis, peristalsis and nanofluids in current biomedical engineering/industry, some mathematical models of fully developed flows driven by the combined outcomes of electroosmotic and peristaltic pumping have been examined for the Newtonian fluid model and nanofluid. However, MHD nanofluids for electroosmotic peristaltic transport for Burgino model have not been taken into account. To fill this research gap, we present a new mathematical model to study the electroosmotic peristaltic pumping analysis of MHD nanofluid in an asymmetric microchannel. Joule heating, viscous dissipation effect and zeta potential of different values are likewise taken in this model. First, the relevant equations for EOF model along the axial electric field have been modeled and then solved for long wavelength and low Reynolds number. Afterwards, the resulting equations are solved numerically by utilizing the Mathematica software. Consequences of pertinent factors on the characteristics of flow, pumping, trapping, and heat transfer have been pointed out.

2 Formulation and solution

Consider a two-dimensional flow $(\tilde{x}, \tilde{y})$ of unsteady magneto-hydrodynamic nanofluid in an asymmetric micro-channel, in which wave propagation is along the $\tilde{x}$ direction

Figure 1 Flow description
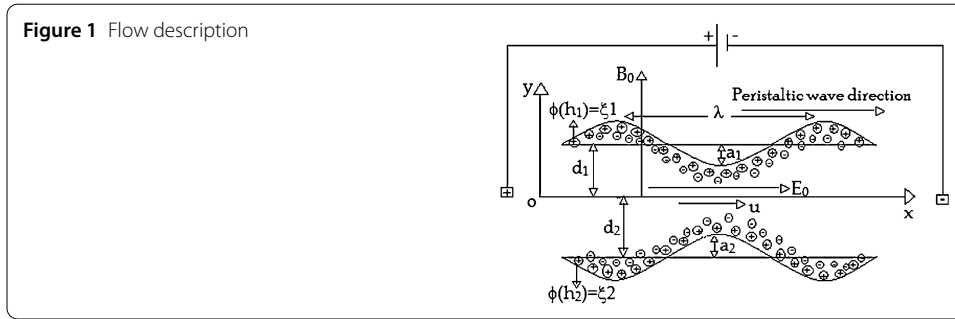
(Fig. 1). This flow is formed by the propagation of a sinusoidal wave at a constant speed c along the channel having elastic walls. The combination of externally applied magnetic field, electric field and pressure gradient affects the driving fluid. It is supposed that the electric field E_0 is imposed axially, and magnetic field B_0 is transversely of the fluid flow. Let $\tilde{y}_1 = \tilde{h}_1(\tilde{x}, \tilde{t})$ and $\tilde{y}_2 = \tilde{h}_2(\tilde{x}, \tilde{t})$ be the upper and lower walls of channel, respectively:

$$\tilde{h}_1(\tilde{x}, \tilde{t}) = d_1 + a_1 \cos^2\left(\frac{(\tilde{x} - c\tilde{t})\pi}{\lambda}\right), \tag{1}$$

$$\tilde{h}_2(\tilde{x}, \tilde{t}) = -d_2 - a_2 \cos^2\left(\frac{(\tilde{x} - c\tilde{t})\pi}{\lambda} + \varphi\right), \tag{2}$$

where $\tilde{h}_1(\tilde{x}, \tilde{y})$, $\tilde{h}_2(\tilde{x}, \tilde{y})$, d_1, d_2, a_1, a_2, φ, λ and $\tilde{t}$ are the upper wall, the lower wall, constant height of upper wall measured from $\tilde{y}_1 = 0$, constant height of lower wall measured from $\tilde{y}_2 = 0$, amplitude of the upper and lower walls, phase difference, wavelength and time, respectively.

2.1 Distribution of potential

Ion separation occurs during EOF, and EDL is formed near the channel walls, creating an electric potential $\tilde{\phi}$ difference. The Poisson–Boltzmann equation is used to describe the $\tilde{\phi}$ in the microchannel:

$$\nabla^2 \tilde{\phi} = -\frac{\rho_e}{\in \in_0}, \tag{3}$$

where ρ_e, $\in$, $\in_0$ and $\tilde{\phi}$ are the net charge density, the relative permittivity of the medium, the permittivity of free space (8.854×10^{-12} F·m^{-1}) and electric potential distribution. The probability of detecting ions at a specific position in electric double layer (EDL) is relative to Boltzmann factor $e^{(ez_v \tilde{\phi}/T_{av}K_B)}$. The positive ($n^+$) and negative ions ($n^-$) can be explained by the number density of the Boltzmann equation:

$$n^{\pm} = n_0 e^{\left(\pm \frac{ez_v}{T_{av}K_B}\tilde{\phi}\right)}, \tag{4}$$

where the average numbers of negative and positive ions are denoted by n_0. The distribution of ionic concentration is considered to be effective when there is no ionic concentration gradient in the axial direction of the microchannel. By the electrolyte symmetry

assumption, the total charge density ρ_e is taken as

$$\rho_e = -z_v e\left(n^- - n^+\right) = -2z_v e n_0 \sinh\left(\frac{e z_v}{T_{av}K_B}\tilde{\phi}\right). \tag{5}$$

In the above, z_v, e, T_{av} and K_B are the ions valence, electron charge, average temperature, and Boltzmann constant. The nonlinear terms in the Nernst–Planck equations are $O(P_e\alpha^2)$, where $P_e = R_e S_c$ represents the ionic Peclet number and S_c is the Schmidt number. Assume that the Peclet number is very small.

Now, by means of Eqs. (3)–(5),we approximate Eq. (3) as:

$$\frac{d^2\tilde{\phi}}{d\tilde{y}^2} = \frac{2z_v e n_0}{\in\in_0}\sinh\left(\frac{e z_v}{T_{av}K_B}\tilde{\phi}\right). \tag{6}$$

The boundary conditions for dimensional form $\tilde{\Phi}$ can be written as

$$\tilde{\phi} = \tilde{\zeta}_1 \quad \text{at } \tilde{y}_1 = \tilde{h}_1(\tilde{x}, \tilde{t}), \tag{7a}$$

$$\tilde{\phi} = \tilde{\zeta}_2 \quad \text{at } \tilde{y}_2 = \tilde{h}_2(\tilde{x}, \tilde{t}), \tag{7b}$$

where $\tilde{\zeta}_1$ and $\tilde{\zeta}_2$ are the zeta potentials at the upper and lower walls, respectively. In order to proceed with dimensionless variables, we introduce:

$$
\begin{aligned}
&a = \frac{d_2}{d_1}, \qquad b = \frac{a_1}{d_1}, \qquad c = \frac{a_2}{d_2}, \qquad h_1 = \frac{\tilde{h}_1}{d_1}, \qquad h_2 = \frac{\tilde{h}_2}{d_1}, \\
&m = \frac{d_1}{\lambda D}, \qquad p = \frac{\tilde{p}d_1^2}{c_\lambda \mu_f}, \qquad t = \frac{c\tilde{t}}{\lambda}, \qquad u = \frac{\tilde{u}}{c}, \qquad v = \frac{\tilde{v}}{c\alpha}, \\
&x = \frac{\tilde{x}}{\lambda}, \qquad y = \frac{\tilde{y}}{d_1}, \qquad B_r = E_c \cdot P_r, \qquad E_c = \frac{c^2}{c_p(T_1 - T_0)}, \\
&H_r = B_0 d_1 \sqrt{\frac{\sigma_e}{\mu_f}}, \qquad N_b = \frac{\gamma 1 (C_1 - C_0)D_B}{v_f}, \\
&N_t = \frac{\gamma_1(T_1 - T_0)D_T}{T_m v_f}, \qquad P_r = \frac{\mu_f c_p}{k_f}, \qquad R_e = \frac{\rho_f c d_1}{\mu_f}, \\
&S_c = \frac{c d_1}{K_B}, \qquad U_{HS} = -\frac{E_0 \in\in_0 T_{av}K_B}{e z_v \mu_f}, \qquad \alpha = \frac{d_1}{\lambda}, \\
&\beta = \frac{U_{HS}}{c}, \qquad \gamma_1 = \frac{(\rho c)_p}{(\rho c)_f}, \qquad \gamma_2 = \frac{\sigma_e d_1^2 E_0^2}{k(T_1 - T_0)}, \qquad \gamma_3 = P_r\gamma_2, \\
&v_f = \frac{\mu_f}{\rho_f}, \qquad \lambda_D = \frac{1}{e z_v}\sqrt{\frac{T_{av}K_B \in\in_0}{2n_0}}, \qquad \zeta_1 = \frac{e z_v}{T_{av}K_B}\tilde{\zeta}_1, \\
&\zeta_2 = \frac{e z_v}{T_{av}K_B}\tilde{\zeta}_2, \qquad \phi = \frac{e z_v}{T_{av}K_B}\tilde{\phi}, \\
&\Theta = \frac{\tilde{T} - T_0}{T_1 - T_0}, \qquad \Omega = \frac{C - C_0}{C_1 - C_0}.
\end{aligned}
\tag{8}
$$

By using the dimensionless variables defined in Eq. (8), Eqs. (6) and (7a)–(7b) become

$$\frac{d^2\phi}{dy^2} = \phi m^2,$$

(9)

$$\phi = \zeta_1 \quad \text{at } y_1 = h_1(x, t),$$

$$\phi = \zeta_2 \quad \text{at } y_2 = h_2(x, t).$$

(10)

Moreover, we suppose that the zeta potential at walls is small enough that the Debye–Hückel linearization is approximately applicable. The linear Poisson–Boltzmann equation is solved by using the boundary conditions given in Eq. (10) to obtain the function of potential distribution

$$\phi = \left(\frac{\zeta_2 \sinh(mh_1) - \zeta_1 \sinh(mh_2)}{\sinh(mh_1 - mh_2)} \right) \cosh(my)$$

$$+ \left(\frac{\zeta_1 \cosh(mh_2) - \zeta_2 \cosh(mh_1)}{\sinh(mh_1 - mh_2)} \right) \sinh(my).$$

(11)

Here, m is the electroosmotic parameter. If we put $\zeta_1 = \zeta_2$, then the solution of Eq. (11) reduces to the results of [8].

2.2 Analysis of flow

Taking into account the viscous dissipation and Joule heating effects, the governing equations for electroosmotically conducting nanofluid affected by the peristaltic flow in asymmetric microchannel are expressed here as:

$$\frac{\partial \tilde{u}}{\partial \tilde{x}} + \frac{\partial \tilde{v}}{\partial \tilde{y}} = 0,$$

(12)

$$\rho_f \left(\frac{\partial \tilde{u}}{\partial \tilde{t}} + \tilde{u}\frac{\partial \tilde{u}}{\partial \tilde{x}} + \tilde{v}\frac{\partial \tilde{u}}{\partial \tilde{y}} \right) = -\frac{\partial \tilde{p}}{\partial \tilde{x}} + \mu_f \left(\frac{\partial^2 \tilde{u}}{\partial \tilde{x}^2} + \frac{\partial^2 \tilde{u}}{\partial \tilde{y}^2} \right) + \rho_e E_0 - \sigma_e B_0^2 \tilde{u},$$

(13)

$$\rho_f \left(\frac{\partial \tilde{v}}{\partial \tilde{t}} + \tilde{u}\frac{\partial \tilde{v}}{\partial \tilde{x}} + \tilde{v}\frac{\partial \tilde{v}}{\partial \tilde{y}} \right) = -\frac{\partial \tilde{p}}{\partial \tilde{y}} + \mu_f \left(\frac{\partial^2 \tilde{v}}{\partial \tilde{x}^2} + \frac{\partial^2 \tilde{v}}{\partial \tilde{y}^2} \right),$$

(14)

$$\left(\frac{\partial \tilde{T}}{\partial \tilde{t}} + \tilde{u}\frac{\partial \tilde{T}}{\partial \tilde{x}} + \tilde{v}\frac{\partial \tilde{T}}{\partial \tilde{y}} \right) = \frac{k_f}{(\rho c)_f} \left(\frac{\partial^2 \tilde{T}}{\partial \tilde{x}^2} + \frac{\partial^2 \tilde{T}}{\partial \tilde{y}^2} \right)$$

$$+ \gamma_1 \left[D_B \left(\frac{\partial \tilde{T}}{\partial \tilde{x}}\frac{\partial \tilde{C}}{\partial \tilde{x}} + \frac{\partial \tilde{T}}{\partial \tilde{y}}\frac{\partial \tilde{C}}{\partial \tilde{y}} \right) + \frac{D_T}{T_m}\left\{ \left(\frac{\partial \tilde{T}}{\partial \tilde{x}} \right)^2 + \left(\frac{\partial \tilde{T}}{\partial \tilde{y}} \right)^2 \right\} \right]$$

$$+ \frac{\Phi}{(\rho c)_f} + \frac{\sigma_e B_0^2 \tilde{u}^2}{(\rho c)_f} + \frac{\sigma_e E_0^2}{(\rho c)_f}.$$

(15)

Here Φ represents the viscous dissipation and is mathematically expressed as:

$$\Phi = \mu_f \left[2\left(\frac{\partial \tilde{u}}{\partial \tilde{x}} \right)^2 + 2\left(\frac{\partial \tilde{v}}{\partial \tilde{y}} \right)^2 + \left(\frac{\partial \tilde{u}}{\partial \tilde{y}} + \frac{\partial \tilde{v}}{\partial \tilde{x}} \right)^2 \right],$$

$$\left(\frac{\partial \tilde{C}}{\partial \tilde{t}} + \tilde{u}\frac{\partial \tilde{C}}{\partial \tilde{x}} + \tilde{v}\frac{\partial \tilde{C}}{\partial \tilde{y}} \right) = D_B \left(\frac{\partial^2 \tilde{C}}{\partial \tilde{x}^2} + \frac{\partial^2 \tilde{C}}{\partial \tilde{y}^2} \right) + \frac{D_T}{T_m}\left(\frac{\partial^2 \tilde{T}}{\partial \tilde{x}^2} + \frac{\partial^2 \tilde{T}}{\partial \tilde{y}^2} \right).$$

(16)

Here $(\tilde{u}, \tilde{v})$ are the components of velocity along the $\tilde{x}$ and $\tilde{y}$ direction, respectively. Also, ρ_f, $\mu_f, \sigma_e, \tilde{p}, \tilde{T}, k_f, (\rho c)_f, \tilde{C}, \gamma_1, D_B$ and D_T represent the density of the fluid, dynamic viscosity of the fluid, electrical conductivity, pressure field, temperature, thermal conductivity of the fluid, heat capacity of the fluid, concentration field, ratio of the effective heat capacity of the nanoparticle to the heat capacity of the fluid, coefficient of thermophoresis diffusion, and coefficient of Brownian motion, respectively. The terms appearing on the left-hand side of Eq. (13) are inertial forces (due to the convection or bulk motion) and the first term on the right-hand side is because of pressure gradient, while the second and third terms are due to viscosity or advection, the fourth term is because of electrical force per unit volume, and the last term is due to magnetic body (per unit volume) forces. Furthermore, the last three terms appearing on the right-hand side of Eq. (15) represent dissipation due to friction, magnetic and electric field, respectively.

Using Eq. (8), the non-dimensional variables, in Eqs. (13)–(16), Eq. (12) is satisfied and Eqs. (13)–(16) become

$$R_e\alpha\left(\frac{\partial}{\partial t} + u\frac{\partial}{\partial x} + v\frac{\partial}{\partial y}\right)u = -\frac{\partial p}{\partial x} + \left(\alpha^2\frac{\partial^2}{\partial x^2} + \frac{\partial^2}{\partial y^2}\right)u + \beta\phi m^2 - H_r^2 u, \tag{17}$$

$$R_e\alpha^3\left(\frac{\partial}{\partial t} + u\frac{\partial}{\partial x} + v\frac{\partial}{\partial y}\right)v = -\frac{\partial p}{\partial y} + \alpha^2\left(\alpha^2\frac{\partial^2}{\partial x^2} + \frac{\partial^2}{\partial y^2}\right)v, \tag{18}$$

$$R_e\alpha\left(\frac{\partial}{\partial t} + u\frac{\partial}{\partial x} + v\frac{\partial}{\partial y}\right)\Theta$$
$$= \frac{1}{P_r}\left(\alpha^2\frac{\partial^2}{\partial x^2} + \frac{\partial^2}{\partial y^2}\right)\Theta + E_c\left[2\alpha^2\left(\frac{\partial u}{\partial x}\right)^2 + 2\alpha^2\left(\frac{\partial v}{\partial y}\right)^2 + \left(\frac{\partial u}{\partial y} + \alpha^2\frac{\partial v}{\partial x}\right)^2\right]$$
$$\quad + \left[N_b\left(\alpha^2\frac{\partial\Omega}{\partial x}\frac{\partial\Theta}{\partial x} + \frac{\partial\Omega}{\partial y}\frac{\partial\Theta}{\partial y}\right) + N_t\left\{\alpha^2\left(\frac{\partial\Theta}{\partial x}\right)^2 + \left(\frac{\partial\Theta}{\partial y}\right)^2\right\}\right]$$
$$\quad + \gamma_2 + E_c H_r^2 u, \tag{19}$$

$$\alpha\left(\frac{\partial}{\partial t} + u\frac{\partial}{\partial x} + v\frac{\partial}{\partial y}\right)\Omega = \frac{1}{S_c}\left(\alpha^2\frac{\partial^2}{\partial x^2} + \frac{\partial^2}{\partial y^2}\right)\Omega + \frac{1}{S_c}\frac{N_t}{N_b}\left(\alpha^2\frac{\partial^2}{\partial x^2} + \frac{\partial^2}{\partial y^2}\right)\Theta. \tag{20}$$

Here, $R_e, \alpha, \beta, H_r, P_r, E_c, N_b, N_t, S_c, \Theta$ and Ω are the Reynolds number, wave number, mobility of the medium, Hartmann number, Prandtl number, Eckert number, thermophoresis parameter, Brownian motion parameter, Schmidt number, dimensionless temperature and concentration field, respectively.

Applying a long-wavelength approximation, ignoring the term with a high power of α, Eqs. (17)–(20) reduce to

$$\frac{\partial p}{\partial x} = \frac{\partial^2 u}{\partial y^2} + \beta\phi m^2 - H_r^2 u, \tag{21}$$

$$\frac{\partial p}{\partial y} = 0, \tag{22}$$

$$\frac{\partial^2\Theta}{\partial y^2} + B_r\left(\frac{\partial u}{\partial y}\right)^2 + P_r N_b\left(\frac{\partial\Omega}{\partial y}\frac{\partial\Theta}{\partial y}\right) + P_r N_t\left(\frac{\partial\Theta}{\partial y}\right)^2 + \gamma_3 + B_r H_r^2 u = 0, \tag{23}$$

$$\frac{1}{S_c}\frac{\partial^2\Omega}{\partial y^2} + \frac{1}{S_c}\frac{N_t}{N_b}\frac{\partial^2\Theta}{\partial y^2} + N_t\left(\frac{\partial\Theta}{\partial y}\right)^2 = 0. \tag{24}$$

By using cross-differentiation, we have eliminated the pressure term from the dimensionless Eqs. (17) and (18), and can write it as a single nonlinear differential equation. Now let us define Ψ, the stream function, as $u = \frac{\partial \Psi}{\partial y}$, $v = -\frac{\partial \Psi}{\partial x}$, satisfying the continuity Eq. (10). Equations (21), (23) and (24) can be expressed as a stream function using:

$$\frac{\partial p}{\partial x} = \frac{\partial^3 \Psi}{\partial y^3} + \beta \phi m^2 - H_r^2 \frac{\partial \Psi}{\partial y}, \tag{25}$$

$$\frac{\partial^4 \Psi}{\partial y^4} - H_r^2 \frac{\partial^2 \Psi}{\partial y^2} + \beta m^2 \frac{\partial \Phi}{\partial y} = 0, \tag{26}$$

$$\frac{\partial^2 \Theta}{\partial y^2} + P_r N_b \left(\frac{\partial \Omega}{\partial y} \frac{\partial \Theta}{\partial y} \right) + P_r N_t \left(\frac{\partial \Theta}{\partial y} \right)^2 + \gamma_3 + B_r \left(\frac{\partial^2 \Psi}{\partial y^2} \right)^2 + H_r^2 B_r \left(\frac{\partial \Psi}{\partial y} \right)^2 = 0, \tag{27}$$

$$\frac{\partial^2 \Omega}{\partial y^2} + \frac{N_t}{N_b} \frac{\partial^2 \Theta}{\partial y^2} = 0. \tag{28}$$

The boundary conditions with Ψ as a stream function are:

$$\frac{\partial \Psi}{\partial y} = 0, \qquad \Psi = \frac{F}{2}, \qquad \Theta = 0, \qquad \Omega = 0 \quad \text{at } y = h_1(x, t), \tag{29a}$$

$$\frac{\partial \Psi}{\partial y} = 0, \qquad \Psi = -\frac{F}{2}, \qquad \Theta = 1, \qquad \Omega = 1 \quad \text{at } y = h_2(x, t). \tag{29b}$$

Here the no slip conditions are imposed at the walls of the channel. Also, we have introduced two extra stream function boundary conditions for the purpose of solving a fourth degree differential equation. The flow rate F in its non-dimensional form is defined as $F = A_0 e^{-Bt}$, where B and A_0 are constants. The negative or positive flow rates are dependent on the value of constant A_0. If $A_0 < 0$ then $F < 0$; similarly, $F > 0$ if $A_0 > 0$. A positive flow rate indicates that the flow is in the direction of peristaltic pumping. Negative flow refers to the opposite of flow and peristaltic motion, also known as reverse pumping. It was experimentally found in [9] that the blood flow rate decreases exponentially with the passage of time. The authors of that paper also depicted that the deviation of blood flow rate is independent on the structural aspects of the microchannel.

3 Solution methodology

The exact solution for above PDEs (25)–(28) along with their related boundary conditions (29a) and (29b) is not possible because the equations are nonlinear and highly coupled. Therefore, solutions to the above equations are computed numerically by utilizing the Mathematica software.

4 Graphical analysis

The effect of appropriate factors on the common outlines (velocity, temperature, and concentration) is graphically discussed in this section. Results of various parameters, for example, Hartmann number H_r, electroosmotic parameter m, the mobility of the medium β, different zeta potentials ζ_1 and ζ_2, Joule heating parameter γ_3, thermophoresis parameter N_t, Brownian motion parameter N_b, Prandtl number P_r and Brinkman number B_r on the flow quantities, i.e., velocity u, temperature θ, concentration Ω and pressure gradient dp/dx, are exhibited in Figs. 2–9.
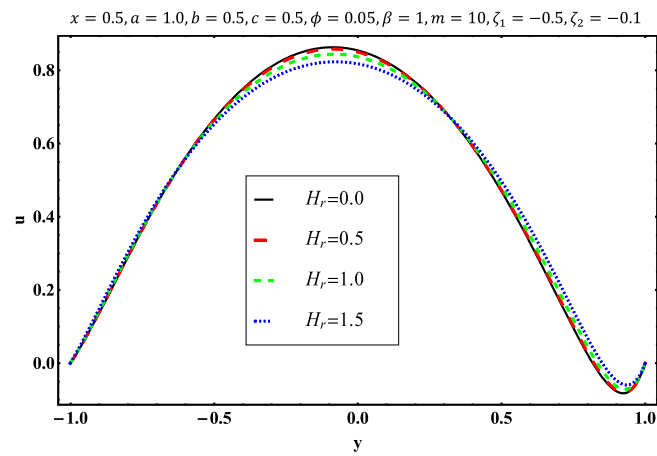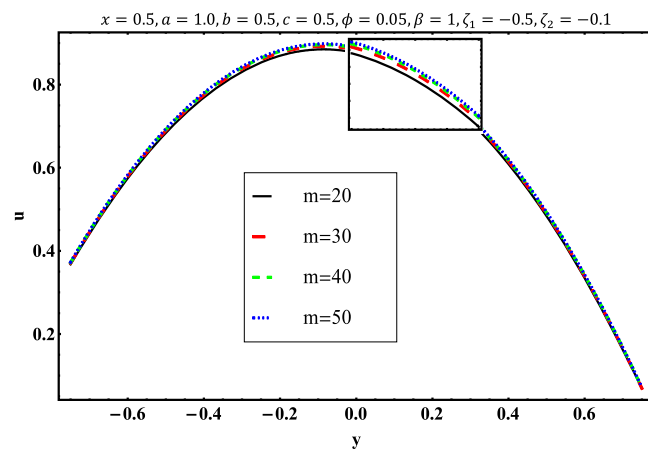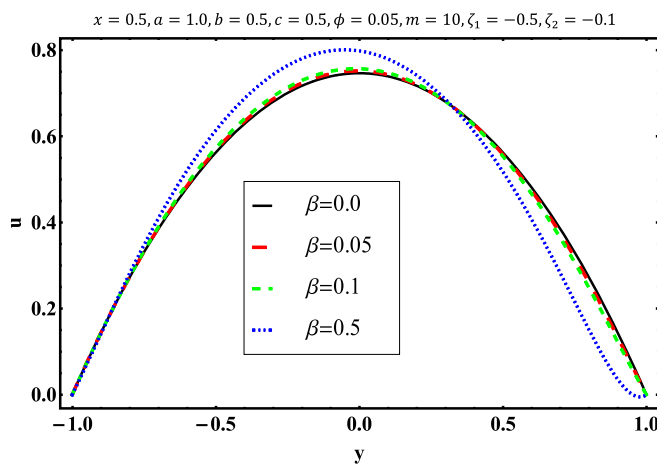
Figure 2 Variation of axial velocity u vs.: (**a**) H_r, (**b**) m, (**c**) β, (**d**) ζ_1, and (**e**) ζ_2.

$x = 0.5, a = 1.0, b = 0.5, c = 0.5, \phi = 0.05, \beta = 1, m = 10, \zeta_2 = -0.1$

Legend:
- $\zeta_1 = -0.1$
- $\zeta_1 = -0.5$
- $\zeta_1 = -1.0$
- $\zeta_1 = -1.5$

(d)

$x = 0.5, a = 1.0, b = 0.5, c = 0.5, \phi = 0.05, \beta = 1, m = 10, \zeta_1 = -0.5$

Legend:
- $\zeta_2 = -0.1$
- $\zeta_2 = -0.5$
- $\zeta_2 = -1.0$
- $\zeta_2 = -1.5$

(e)

Figure 2 Continued
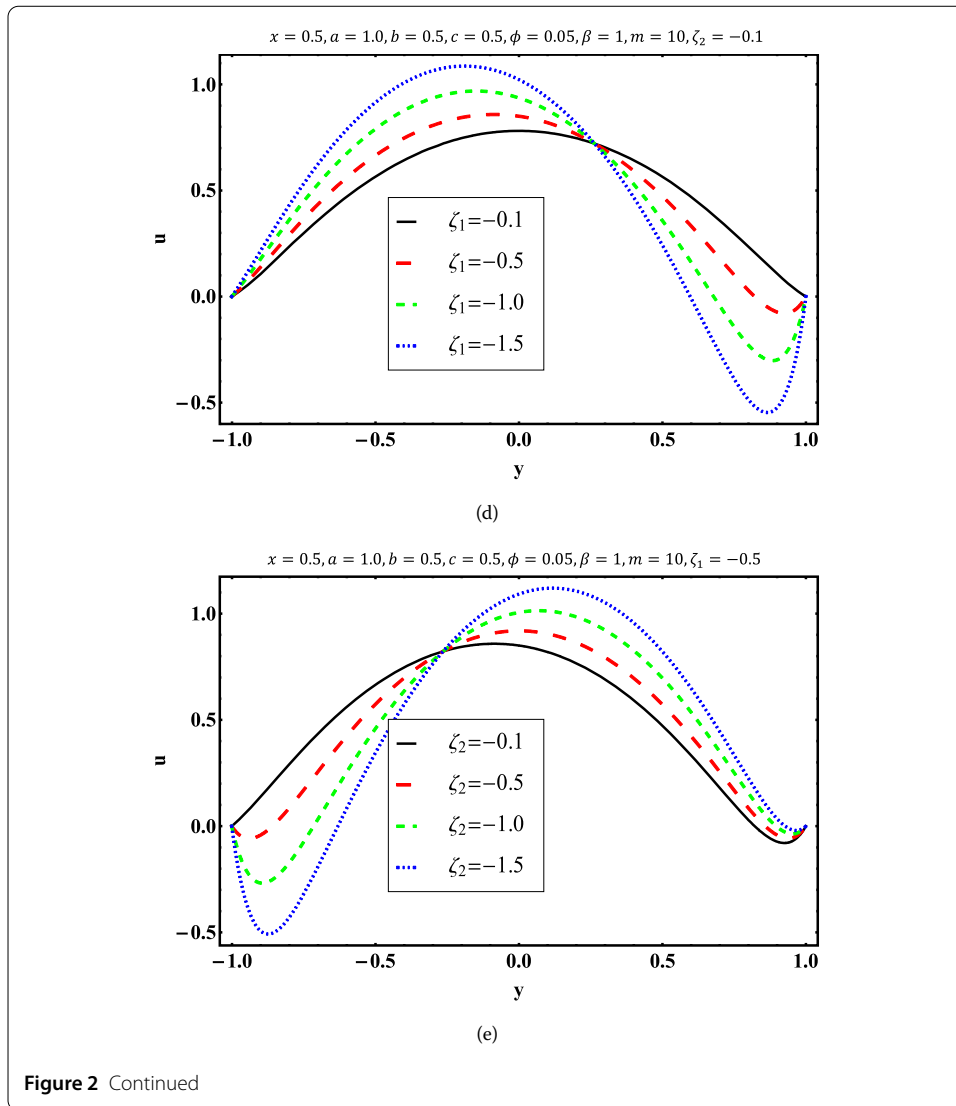
4.1 Characteristics of flow

This subsection explains the detailed analysis of velocity distribution. Figures 2(a)–(e) have been plotted to observe the changes in velocity profile, across the microfluidic channel under the influence of Hartmann number H_r, electroosmotic parameter m, the mobility of the medium β, zeta potentials ζ_1 and ζ_2. Figure 2(a) demonstrates that the velocity (axial) decreases in the central region of the channel as H_r increases, whilst the reverse trend is viewed near the channel walls because decrease in axial velocity subject to increase in magnetic field strength. Since magnetic field and axial velocity are perpendicular to each other, they produce a Lorentz force, which has a propensity to slow the movement of the fluid. Thus, the (axial) velocity has a rapid acceleration effect for H_r in the middle area of the channel and reduces close to the channel wall. Figure 2(b) shows an increased behavior for the subregion $-0.1 \leq y \leq 0.1$. Since m is the fraction of the conduit height to the λ_D, it signifies that the increase of λ_D leads to a decrease in EDL, so that a large amount of fluid rapidly flows in the central region. Figure 2(c) portrays that the (axial) velocity increases as the mobility of the medium in the middle region of the conduit increases,

Figure 3 Pressure gradient distribution vs. (**a**) H_r, (**b**) m, (**c**) β, (**d**) ζ_1, and (**e**) ζ_2.
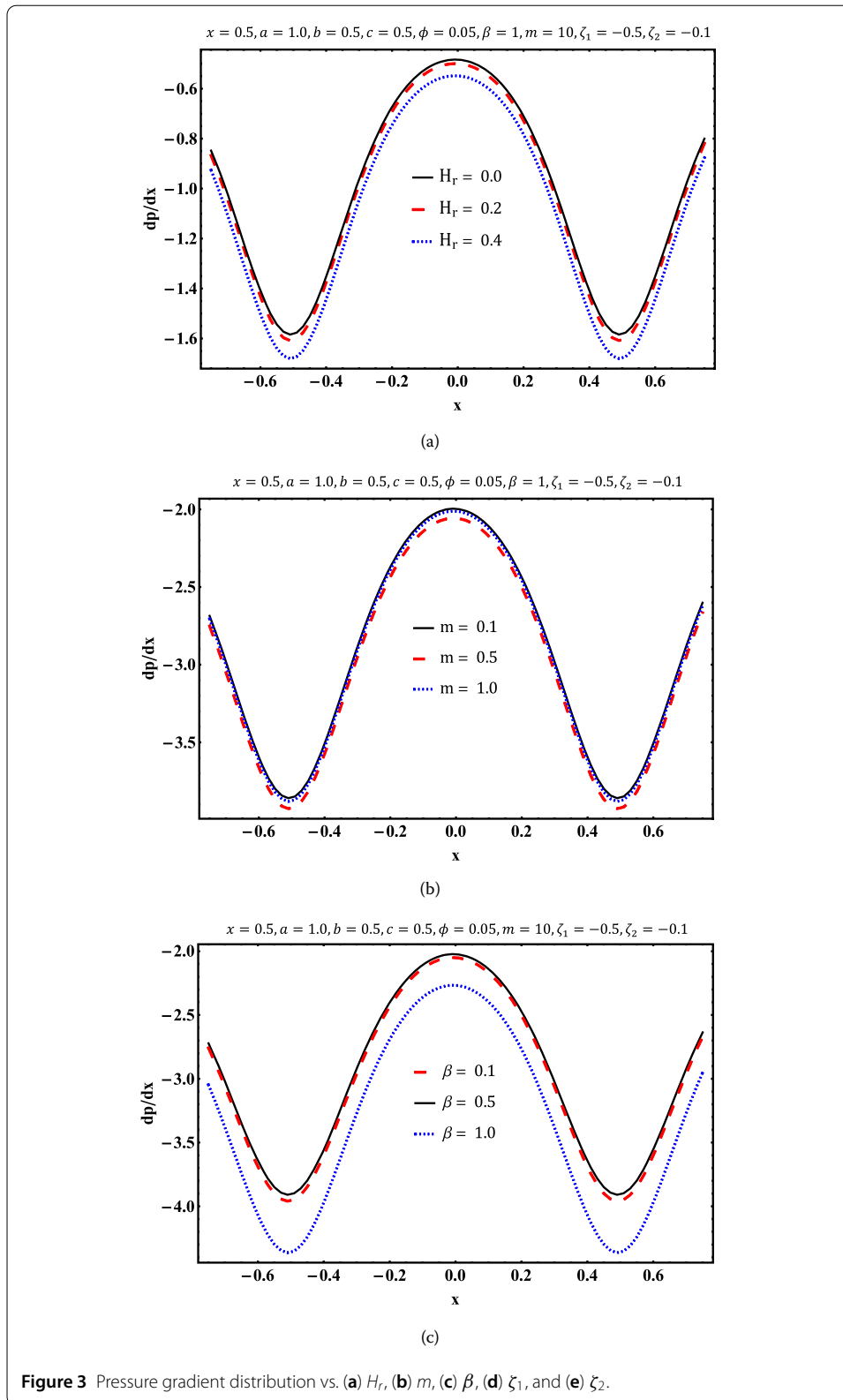
while decreasing in the left region of the conduit, because β is directly dependent on the Helmholtz–Smoluchowski velocity U_{HS}. This physically can be interpreted as follows: the

$x = 0.5, a = 1.0, b = 0.5, c = 0.5, \phi = 0.05, \beta = 1, m = 10, \zeta_2 = -0.1$

(d)

$x = 0.5, a = 1.0, b = 0.5, c = 0.5, \phi = 0.05, \beta = 1, m = 10, \zeta_1 = -0.5$

(e)

Figure 3 Continued
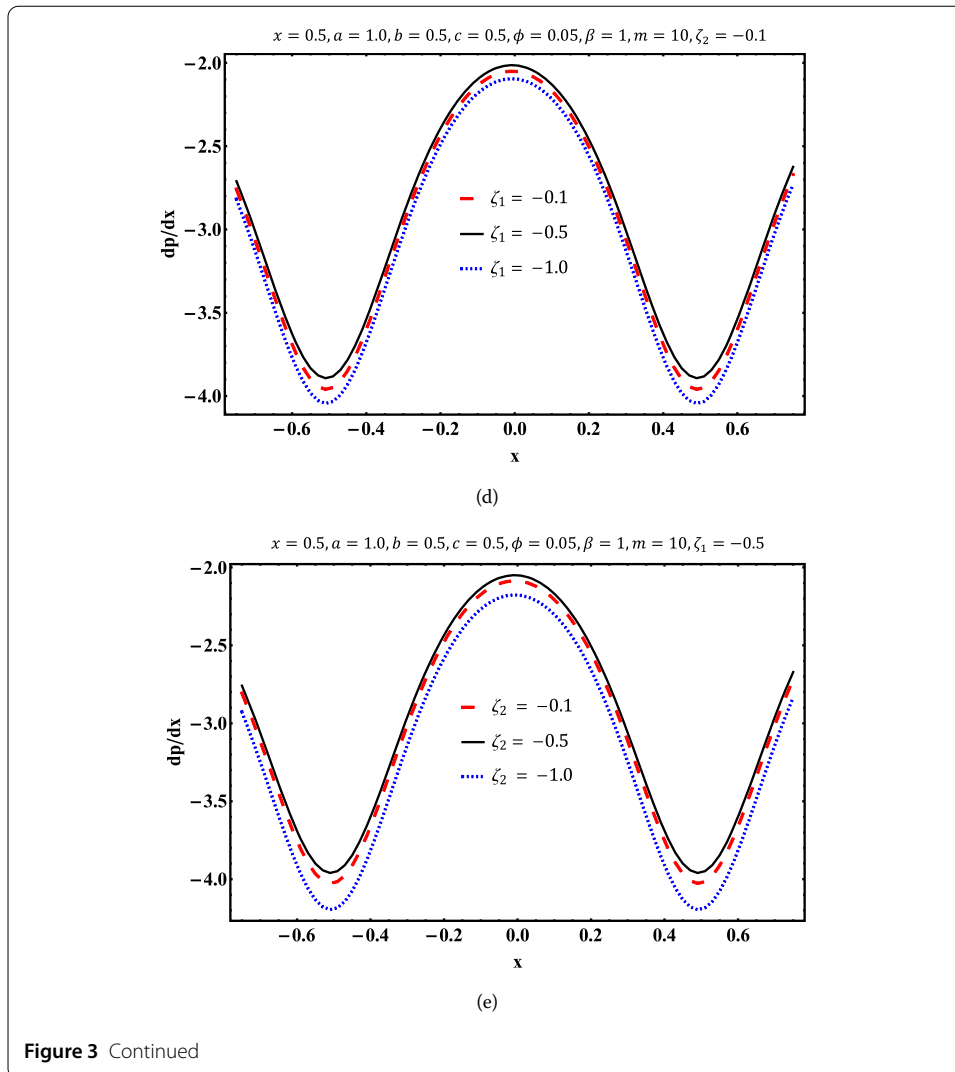
velocity of fluid reduces with increasing thickness of EDL and the flow of fluid reduces in the presence of EDL. Figure 2(d) shows the effect of (axial) velocity distribution with respect to ζ_1 on the upper microchannel wall. It is also observed that the change in ζ_1 significantly enhances the axial velocity distribution of the EOF. As the zeta potential behavior of the upper wall increases, the velocity has an increased effect on the lower wall, while the opposite behavior is observed at the upper wall of the channel. In Fig. 2(e), a parallel behavior of velocity distribution is observed due to the zeta potential ζ_2. For different values of ζ_1 and ζ_2, the intersection summit is not completely in the middle of the channel walls. Clearly, a higher value of the zeta potential produces a strong field of EDL and thus a decrease in the fluid velocity. This zeta potential phenomenon produces different rates of flow at different locations in the microchannel, thus changing the momentum flux. The presence of zeta potential in an EOF is a key phenomenon in controlling fluid flow in the microchannel. We examined that our results are consistent with previous studies without zeta potential [11].

Figure 4 Streamline distribution for; (**a**) $H_r = 0.0$, (**b**) $H_r = 1.5$, and (**c**) $H_r = 3.0$.
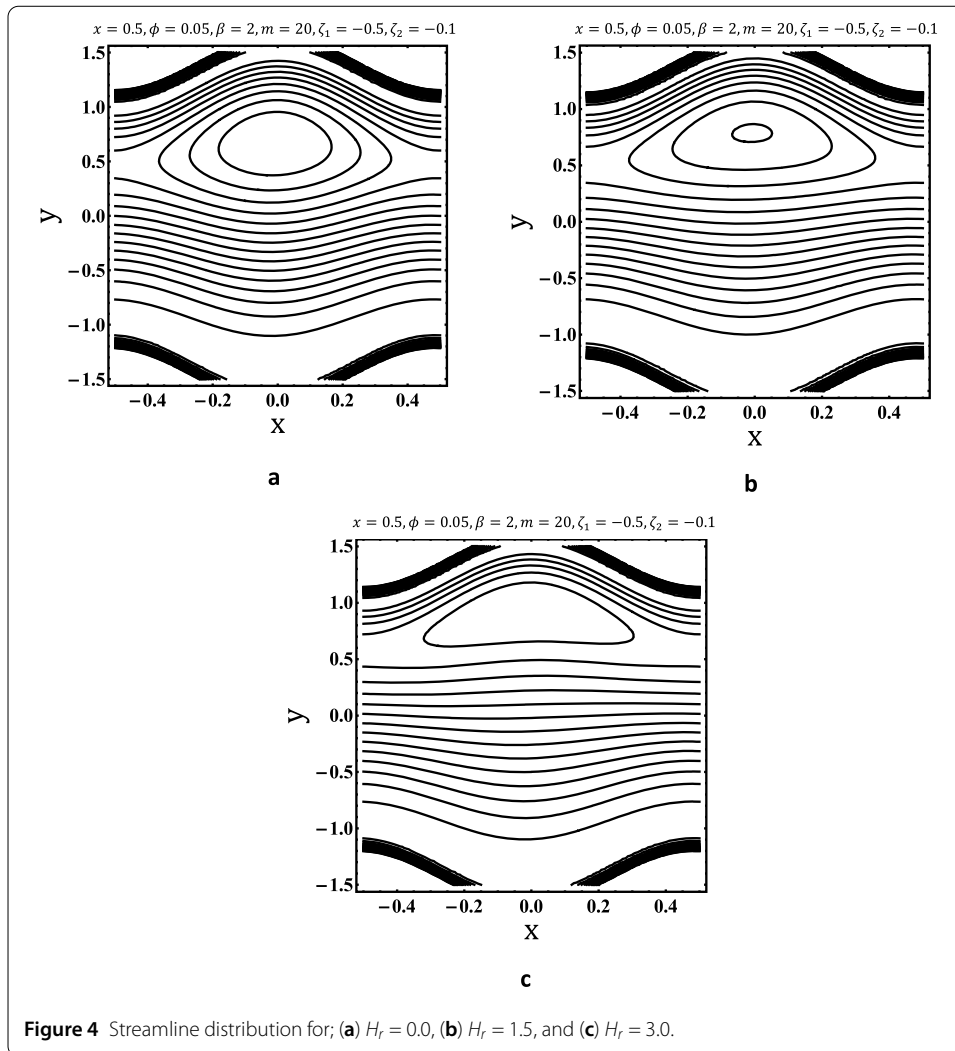
4.2 Characteristics of pumping

It is clear that the transport in the peristalsis is related to the perception of mechanical pumping. Consequently, it is justifiable to study the pumping behavior from the current research perceptive. Figure 3(a) highlights that by increasing the Hartmann number H_r, pressure gradient magnitude increases. As H_r is the fraction of Lorentz force (electromagnetic force) to viscous force, higher values of Hartmann number indicate stronger Lorentz force, hence more pressure is needed to overcome the Lorentz force. Figure 3(b) shows that by raising the value of m, the magnitude of pressure gradient increases. Likewise, it is worth noting that the pumping features can be amended by the EDL phenomenon, and the pumping procedure can be organized by thickening and thinning the breadth of EDL. Similarly, by increasing the value of the mobility of the medium β, the magnitude of the pressure gradient increases as shown in Fig. 3(c). Figures 3(d) and 3(e) also explain the impact of the zeta potentials ζ_1 and ζ_2 on the axial pressure gradient. It is also determined that the pressure gradient declines significantly then increasing the zeta potential of the upper and lower walls of the channel.

Figure 5 Streamline distribution for: (**a**) $\beta = 0.0$, (**b**) $\beta = 0.5$, and (**c**) $\beta = 1.0$.
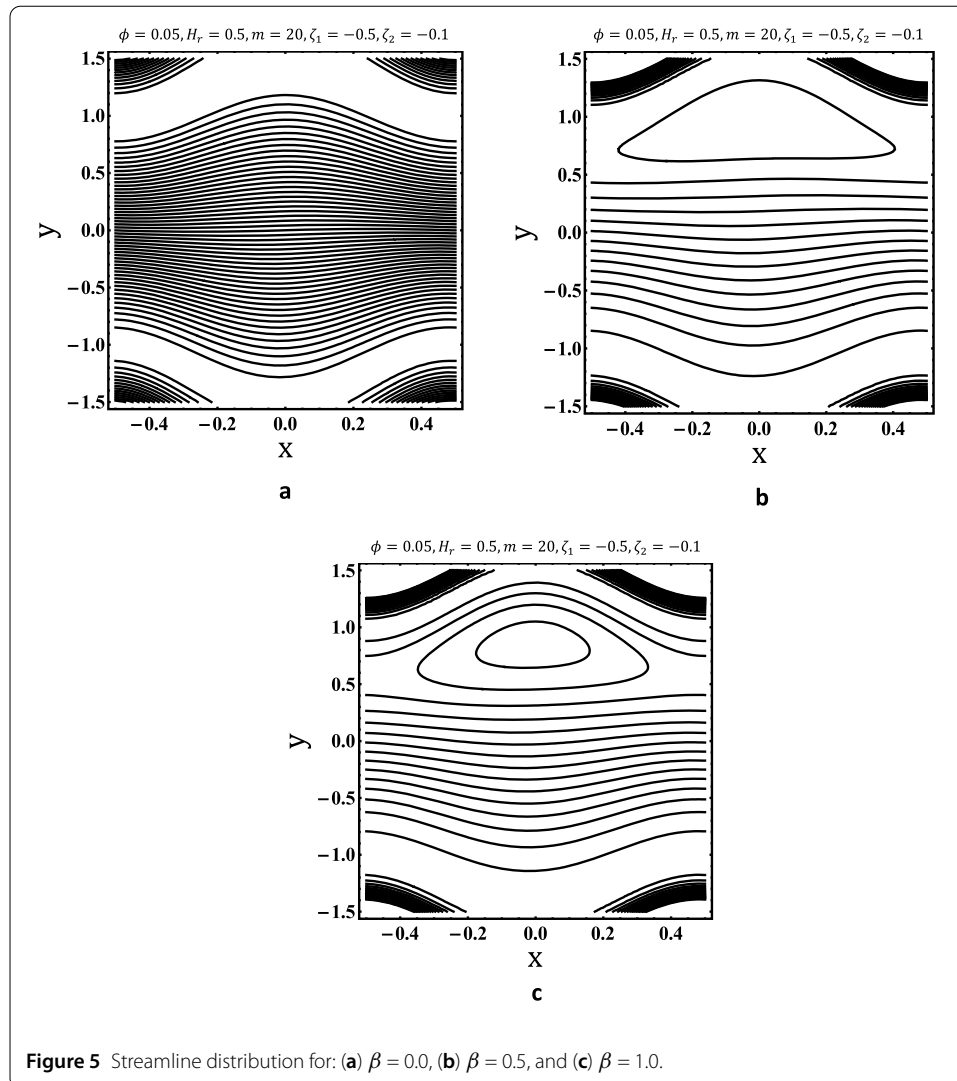
4.3 Characteristics of trapping

Trapping is a peristaltic pumping mechanism, in which a flow streamline forms a circular path, which is called a bolus at volumetric flow rate value. Figures 4–6 give an insight into streamline structural changes that happen due to H_r value, the mobility of the medium β and the change in the electroosmotic parameter m on the microfluidic channel. They also illustrate that bolus formation occurs near the central line of the channel. Furthermore, it is shown that the size of trapped bolus first decreases while the strength of magnetic field increases and disappears for a sufficient magnetic field strength. Moreover, it can be noted that a higher zeta is applied at the upper wall than at the lower wall whereas the streamline is significantly circulated at the upper wall. Similarly, Figs. 7(a)–(c) depict that the number of trapped bolus increases on the upper wall. Figures 8(a)–(c) show that the number of trapped bolus increases on the lower wall but decreases on the upper wall. Figures 4–8 demonstrate that the accumulation of streamline is far away from the center due to strong EDL. It is concluded that as the zeta potential increases, the width of the EDL also increases. Thus, the streamline strongly forms a closed region and is transmitted at a

Figure 6 Streamline distribution for: (**a**) $m = 5.0$, (**b**) $m = 10$, and (**c**) $m = 15$.
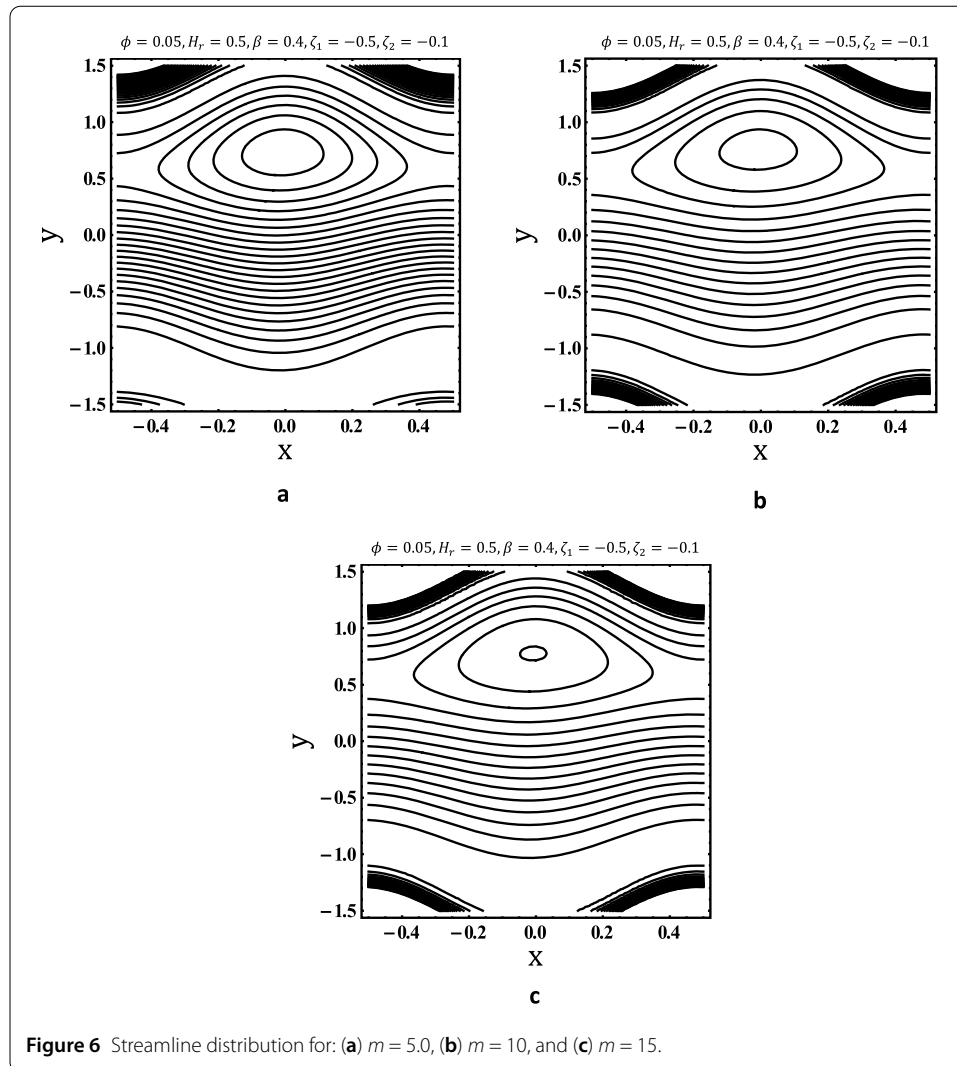
wave velocity in the frontward direction. This phenomenon will help enhance the flow in the microfluidic device.

4.4 Heat and concentration characteristics

The generation of Joule heating during electroosmotic stream is a built-in characteristic. However, this effect is caused by the electrical resistance, which is produced by the electrolyte. Figures 9–14 explain the various values of Joule heating parameter γ_3, electroosmotic parameter m, Brinkman number B_r, Hartmann number H_r, Prandtl number P_r, Brownian motion parameter N_b, and thermophoresis parameter N_t. Figure 9(a) shows that temperature increases very quickly in the central area of the channel by increasing the values of Joule heating parameter γ_3, whereas it is insignificant near the channel walls. Joule heating parameter γ_3 is directly proportional to the square of the electric field, hence a stronger electric field results in a rise in the temperature, while concentration Ω falls with the increase in γ_3 as shown in Fig. 9(b). Figure 10(a) illustrates the effect of the Brinkman number B_r on the temperature distribution near the middle section of the conduit. Though B_r is the ratio of viscous dissipation to molecular conductivity, a higher the B_r value low-
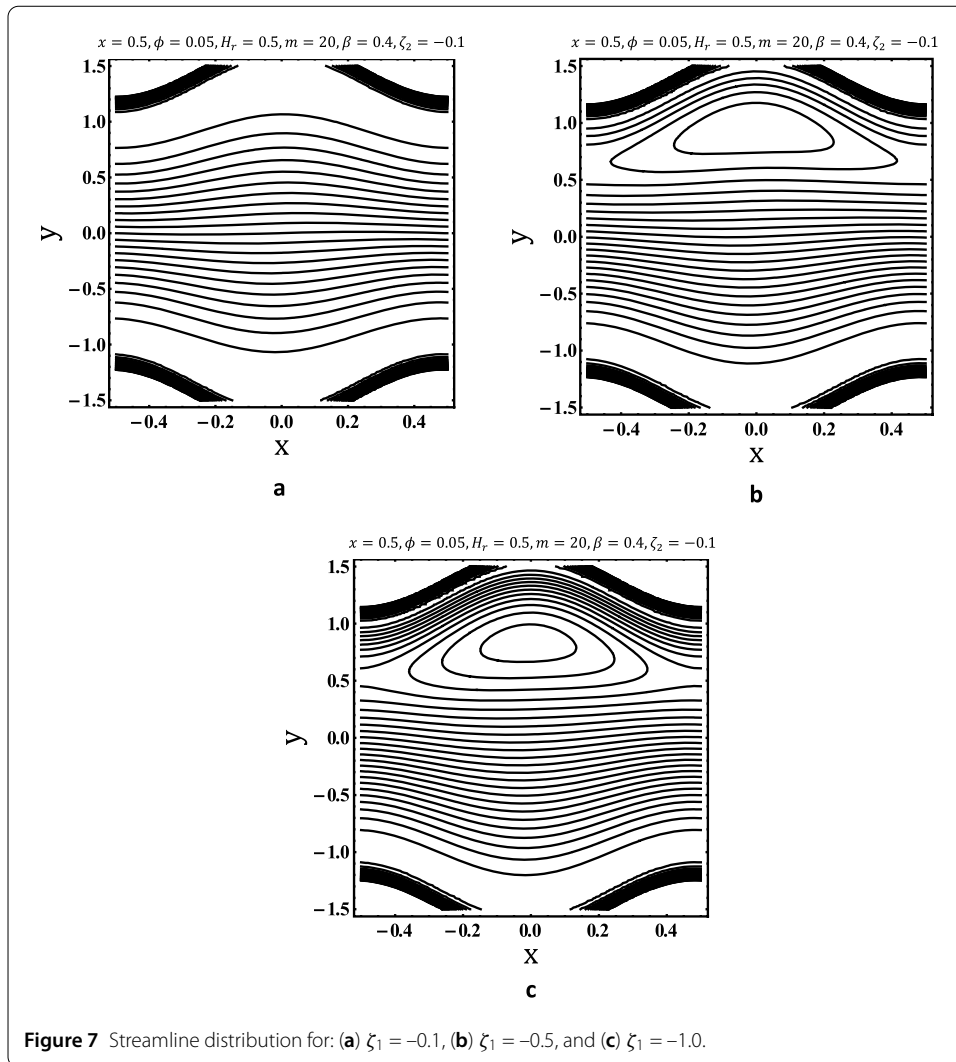
Figure 7 Streamline distribution for: (**a**) $\zeta_1 = -0.1$, (**b**) $\zeta_1 = -0.5$, and (**c**) $\zeta_1 = -1.0$.

ers the conduction of heat due to viscous dissipation. Thus, temperature rises remarkably. Physically, the dominating aspect in B_r is viscosity, due to which resistance is produced. This resistance causes fluid particles to collide, and the collision of fluid particles is responsible for increase in the temperature, whereas Fig. 10(b) shows that concentration declines due to increasing behavior of B_r. Variation in temperature distribution against different values of Hartmann number H_r can be observed in Fig. 11(a). It signifies that the temperature increases when increasing Hartmann number, and the converse is shown for concentration in Fig. 11(b). This rise is more significant in the central area of the channel for higher values of H_r because H_r describes the Lorentz forces, which are resistive forces; they are used here to control the turbulence in the fluid flow. Figure 12(a) shows the effects of P_r on the temperature distribution. This P_r is directly proportional to viscosity and specific heat, and inversely proportional to thermal conductivity. It is observed that the magnitude of the Prandtl number increases due to temperature, i.e., P_r has increased due to the distribution of temperature which is shown in the middle area of the conduit. Physically, the temperature is strongly dependent on thermal and momentum diffusivity. Although for concentration, the reverse trend is scrutinized in Fig. 12(b). It signifies that

Figure 8 Streamline distribution for: (**a**) $\zeta_2 = -0.1$, (**b**) $\zeta_2 = -0.5$, and (**c**) $\zeta_2 = -1.0$.
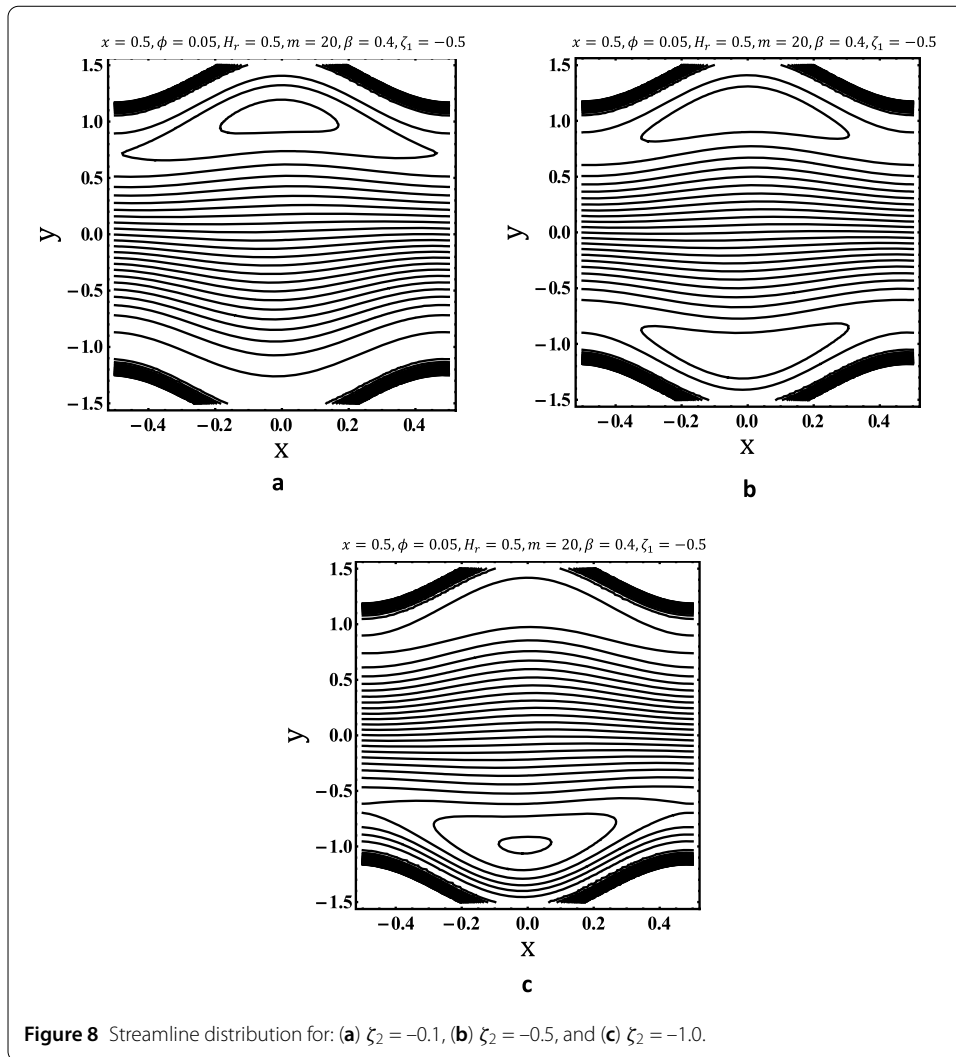
P_r is directly proportional to viscosity. As viscosity decreases, P_r decreases. Therefore, concentration decreases for increasing values of P_r. Figure 13(a) illustrates that the temperature increases as the magnitude of N_b increases, since N_b plays an accelerating role on temperature profile. This situation arises due to random motion of molecules, and temperature profile increases. Similarly, concentration increases as N_b increases in Fig. 13(a), since N_b is directly proportional to concentration gradient and inversely proportional to viscosity and diffusion coefficient. It shows that as N_b increases, the diffusion coefficient decreases, so concentration gradient increases. Therefore, concentration profile increases. Figure 14(a) shows that the temperature distribution rises as N_t increases, since N_t is directly proportional to temperature gradient. As N_t increases, temperature gradient also increases due to increase in internal energy. Therefore, temperature profile increases. On the other hand, Fig. 14(b) illustrates that the concentration decreases due to an increase in N_t, because when temperature increases, the number of collisions of particles increases. Due to these collisions, concentration of fluid is disturbed. Thus, concentration decreases. Our work has achieved better approximations compared to [7].

Figure 9 For different values of γ_3 (**a**), temperature distribution Θ (**b**) and concentration distribution Ω.
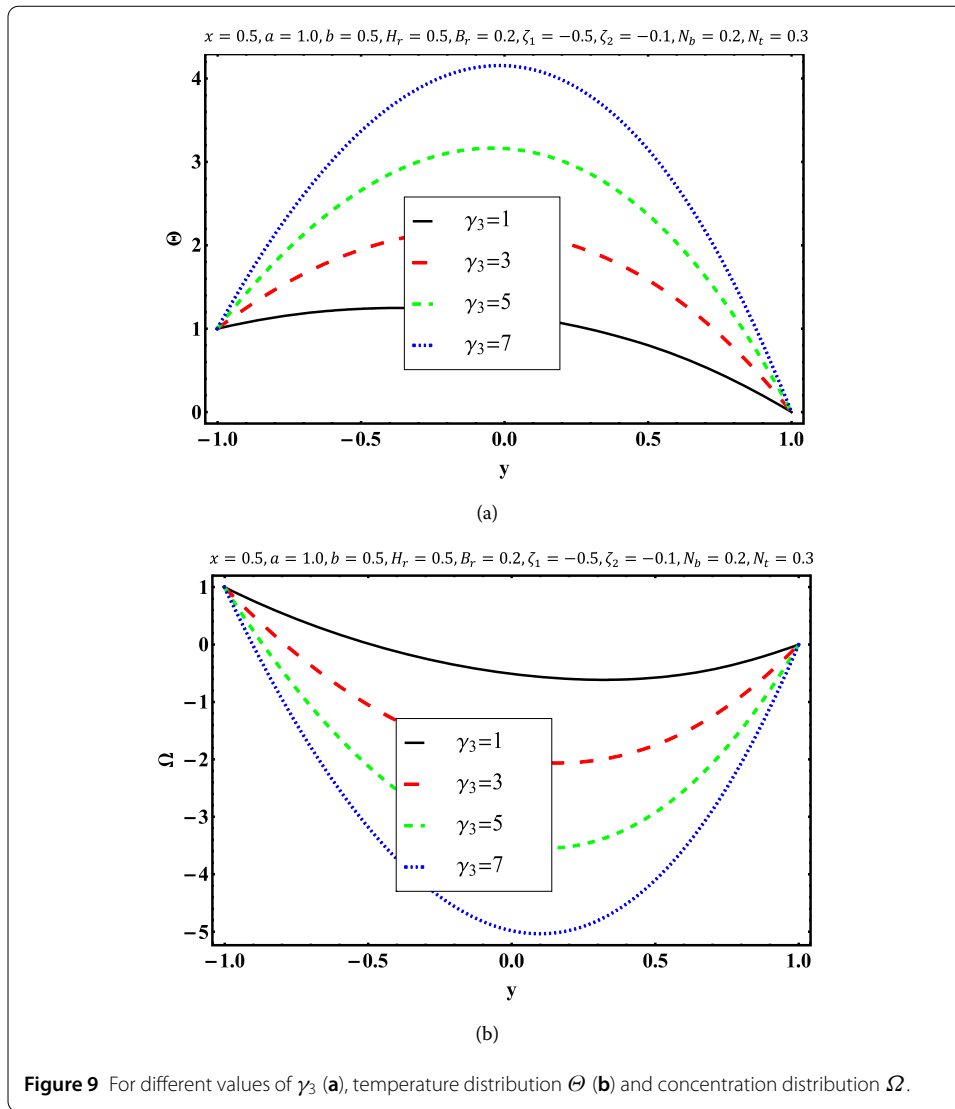
5 Summary and conclusions

The purpose of this study was to investigate the electroosmotic peristaltic pumping of MHD nanofluid in an asymmetric microfluidic channel with zeta potentials. Joule heating and viscous dissipation effects were likewise considered in this model. Suitable boundary conditions have been utilized to get the solution for highly nonlinear and coupled PDEs. The significant results of this study are summarized as follows:

- The (axial) velocity increases in the middle section of the channel, with a reduction in the vicinity due to electroosmotic parameter and mobility of the medium.
- The magnitude of axial pressure gradient firstly decreases then increases with the increase of electroosmotic parameter, Hartmann number, mobility of the medium and different zeta potentials.
- Since a higher potential is applied at the upper wall than at the lower wall, streamline circulates significantly close to that wall where potential is high.
- The construction of trapped bolus depends strongly on the electroosmotic parameter, Hartmann number, mobility of the medium and high zeta potentials.
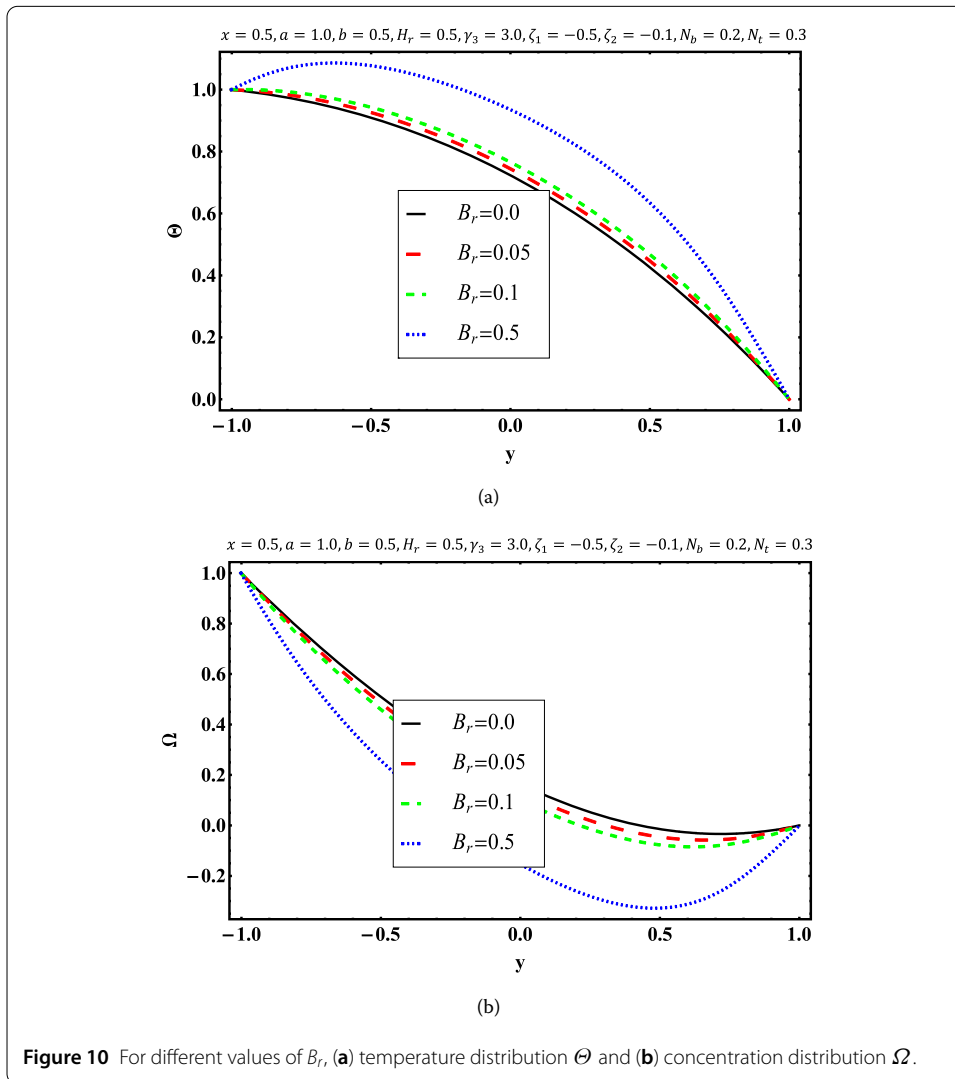
Figure 10 For different values of B_r, (**a**) temperature distribution Θ and (**b**) concentration distribution Ω.
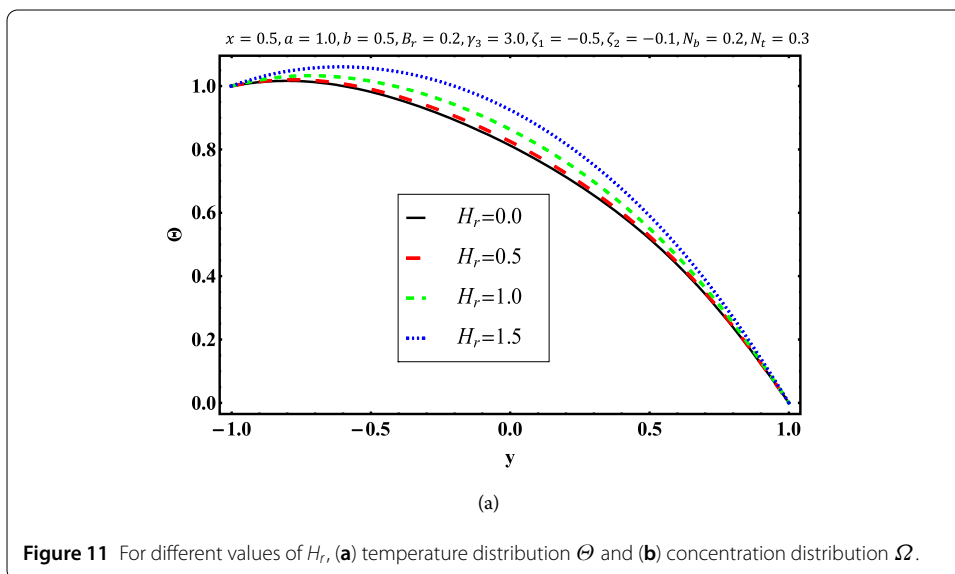
Figure 11 For different values of H_r, (**a**) temperature distribution Θ and (**b**) concentration distribution Ω.

$x = 0.5, a = 1.0, b = 0.5, B_r = 0.2, \gamma_3 = 3.0, \zeta_1 = -0.5, \zeta_2 = -0.1, N_b = 0.2, N_t = 0.3$

(b)

Figure 11 Continued

$x = 0.5, a = 1.0, b = 0.5, H_r = 0.5, \gamma_3 = 3.0, \zeta_1 = -0.5, \zeta_2 = -0.1, N_b = 0.2, N_t = 0.3$

(a)

$x = 0.5, a = 1.0, b = 0.5, H_r = 0.5, \gamma_3 = 3.0, \zeta_1 = -0.5, \zeta_2 = -0.1, N_b = 0.2, N_t = 0.3$

(b)
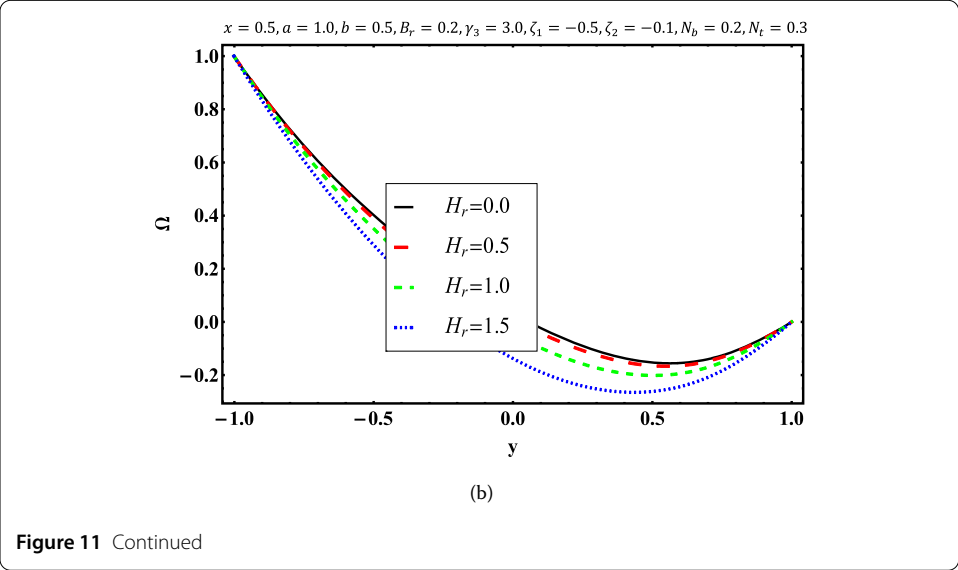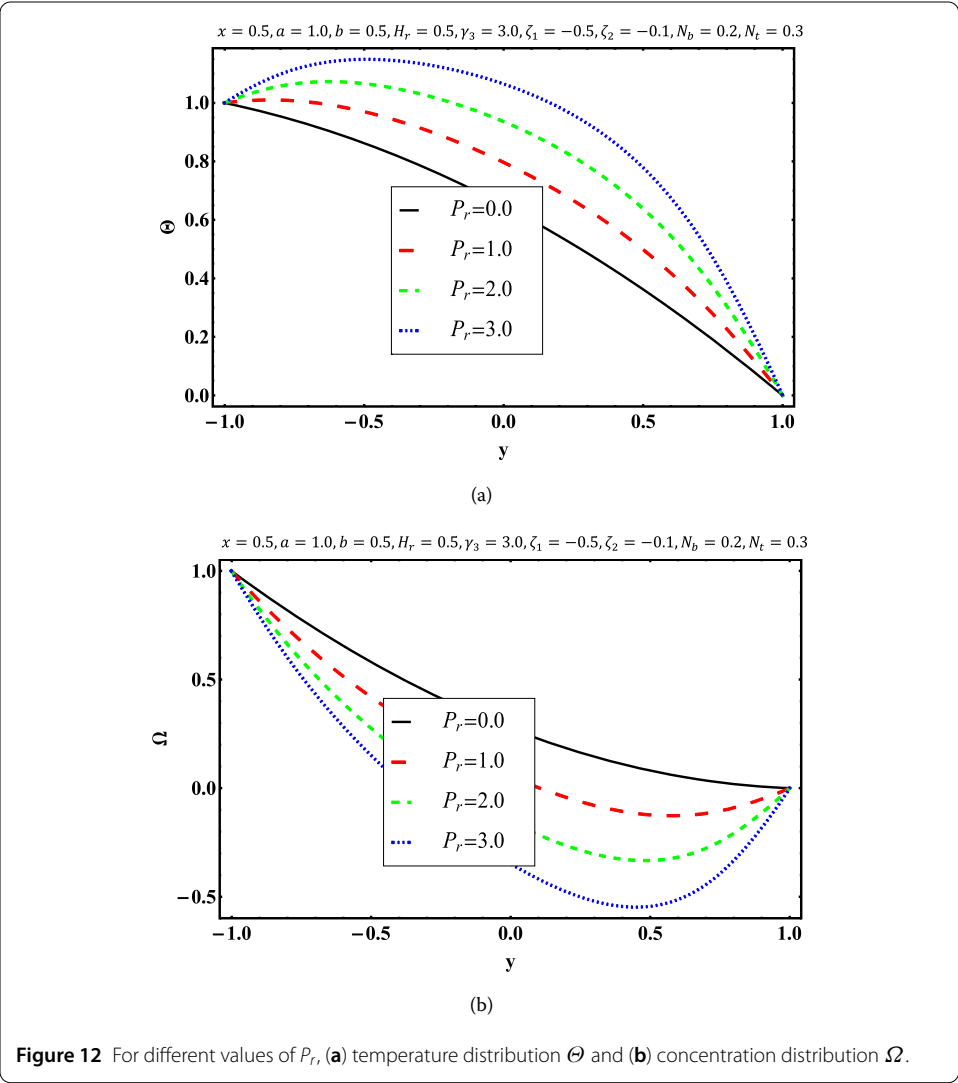
Figure 12 For different values of P_r, (**a**) temperature distribution Θ and (**b**) concentration distribution Ω.

$x = 0.5, a = 1.0, b = 0.5, P_r = 1.2, H_r = 0.5, \gamma_3 = 3.0, \zeta_1 = -0.5, \zeta_2 = -0.1, N_t = 0.3$

(a)

$x = 0.5, a = 1.0, b = 0.5, P_r = 1.2, H_r = 0.5, \gamma_3 = 3.0, \zeta_1 = -0.5, \zeta_2 = -0.1, N_t = 0.3$

(b)
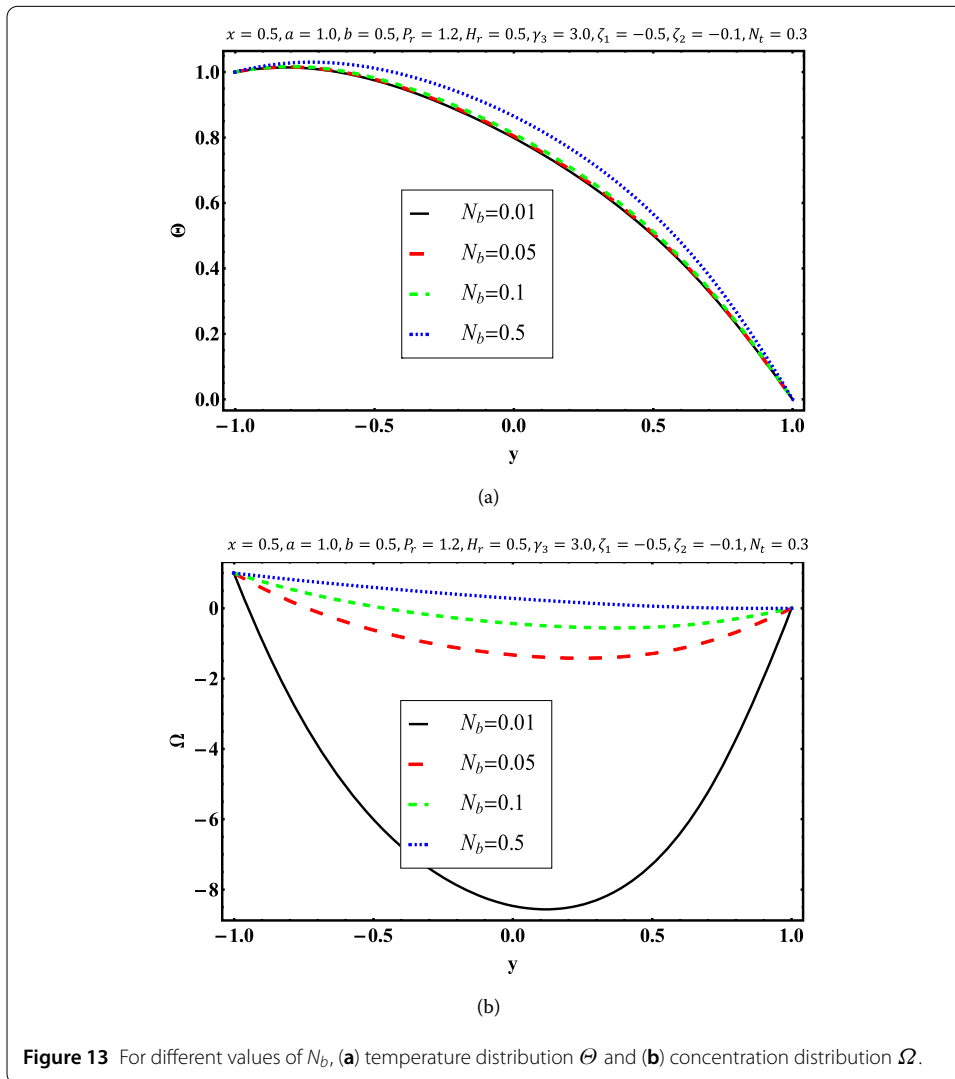
Figure 13 For different values of N_b, (**a**) temperature distribution Θ and (**b**) concentration distribution Ω.

$x = 0.5, a = 1.0, b = 0.5, P_r = 1.2, H_r = 0.5, \gamma_3 = 3.0, \zeta_1 = -0.5, \zeta_2 = -0.1, N_b = 0.2$

(a)
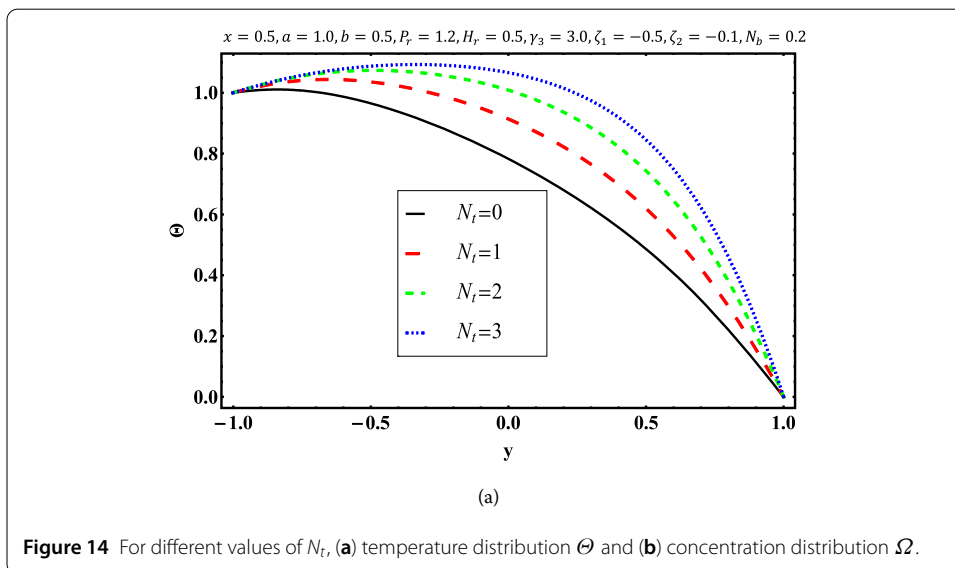
Figure 14 For different values of N_t, (**a**) temperature distribution Θ and (**b**) concentration distribution Ω.

Figure 14 Continued
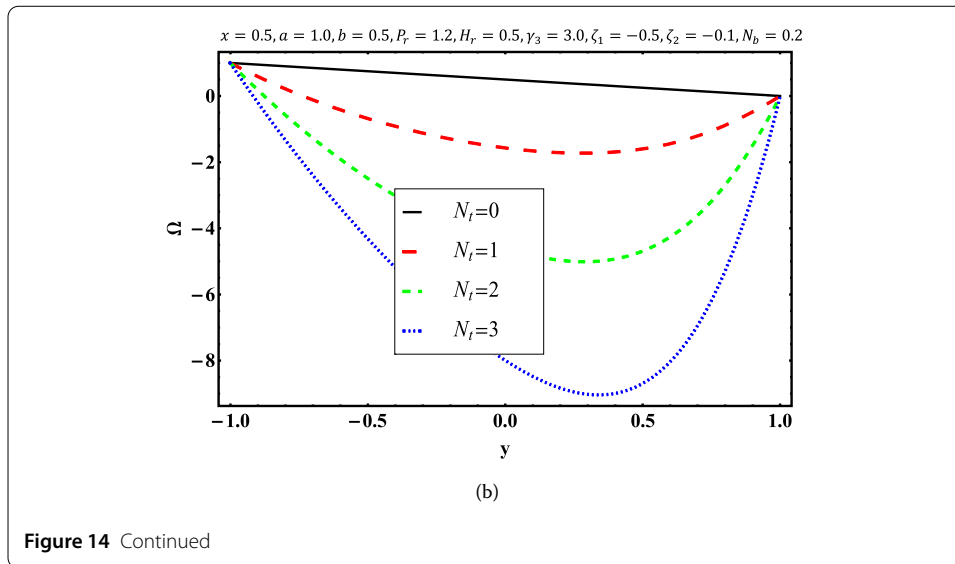
- The heat transfer rate impacts the energy dissipation caused by the existence of Joule heating impact.

Nomenclature
a_1, a_2, Amplitude of upper and lower wall [L]; B_0, Magnetic field [A/L]; B_r, Brinkman number [–]; c, Wave speed [L/T]; C, Dimensional concentration field; C_0, C_1, Concentrations of fluid at upper and lower walls; c_f, Specific heat [ML^2/T^{2}K]; c_p, Heat capacity of fluid [ML^2/T^{2}K]; d_1, d_2, Constant heights [L]; D_T, Coefficient of thermophoresis diffusion; D_B, Coefficient of Brownian motion; e, Electron charge [C]; E_0, Electric field [M/T^{3}A]; E_c, Eckert number [–]; F, Flow rate [L^3/T]; $\tilde{h}_1$, $\tilde{h}_2$, Dimensional upper and lower walls [L]; h_1, h_2, Non-dimensional upper and lower walls [–]; H_r, Hartmann number [–]; K_B, Boltzmann constant; k_f, Thermal conductivity of fluid [ML/T^{3}K]; m, Electroosmotic parameter; $n^\pm$, Positive, negative ions; n_0, Average number of n^+ or n^- ions; N_b, Brownian motion parameter; N_t, Thermophoresis parameter; $\tilde{p}$, Pressure field [ML/T^2]; p, Pressure field [–]; P_r, Prandtl number [–]; R_e, Reynolds number [–]; S_c, Schmidt number [–]; $\tilde{t}$, Dimensional time [T]; t, Dimensionless time [–]; $\tilde{T}$, Temperature field [K]; T_0, T_1, Temperatures of fluid at upper and lower walls [K]; U_{HS}, Helmholtz–Smoluchowski velocity; $\tilde{u}$, $\tilde{v}$, Dimensional velocity components in stationary frame [L/T]; u, v, Non-dimensional velocity components in wave frame [–]; $\tilde{x}$, $\tilde{y}$, Dimensional coordinates in stationary frame [L]; x, y, Non-dimensional coordinates in wave frame [–]; z_v, Valence of ions; α, Wave number [–]; β, Mobility of the medium; γ_1, Ratio of the effective heat capacity of the nanoparticle to the heat capacity of the fluid [–]; γ_3, Joule heating parameter [–]; ϵ_0, Permittivity of free space [–]; ϵ, Relative permittivity of the medium [–]; $\tilde{\zeta}_1$, $\tilde{\zeta}_2$, Dimensional upper and lower wall zeta potential; ζ_1, ζ_2, Non-dimensional upper and lower wall zeta potential; $\Theta(y, t)$, Temperature field [K]; λ, Wave length of peristaltic wave [L]; λ_D, Debye length; μ_f, Dynamic viscosity of fluid [M/LT]; ρ_f, Density of fluid [M/L^3]; ρ_e, Net ionic charge density [M/L^3]; $(\rho c)_p$, $(\rho c)_f$, Heat capacity of the nanoparticles and the base fluid [ML^2/T^{2}K]; σ_e, Electrical conductivity [T^{3}I^2/L^{3}M]; $\tilde{\phi}$, Dimensional electric potential distribution [ML^2/T^{2}I]; ϕ, Non-dimensional electric potential distribution [–]; φ, Phase difference [L]; Ψ, Dimensional Stream function [L^2/T]; Ω, Non-dimensional concentration field [–].

Author details
[1]Department of Mathematics, Comsats University Islamabad, Islamabad, Pakistan. [2]Division of Computational
Mathematics and Engineering, Institute for Computational Science, Ton Duc Thang University, Ho Chi Minh City, Vietnam.
[3]Faculty of Mathematics and Statistics, Ton Duc Thang University, Ho Chi Minh City, Vietnam.

Publisher's Note
Springer Nature remains neutral with regard to jurisdictional claims in published maps and institutional affiliations.

References

1. Bandopadhyay, A., Tripathi, D., Chakraborty, S.: Electroosmosis-modulated peristaltic transport in microfluidic channels. Phys. Fluids **28**(5), 052002 (2016)
2. Shit, G.C., Mondal, A., Sinha, A., Kundu, P.K.: Effects of slip velocity on rotating electro-osmotic flow in a slowly varying micro-channel. Colloids Surf. A, Physicochem. Eng. Asp. **489**, 249–255 (2016)
3. Tripathi, D., Bhushan, S., Bég, O.A.: Unsteady viscous flow driven by the combined effects of peristalsis and electro-osmosis. Alex. Eng. J. (2017)
4. Ranjit, N.K., Shit, G.C.: Joule heating effects on electromagnet hydrodynamic flow through a peristaltically induced micro-channel with different zeta potential and wall slip. Phys. A, Stat. Mech. Appl. **482**, 458–476 (2017)
5. Tripathi, D., Jhorar, R., Bég, O.A., Shaw, S.: Electroosmosis modulated peristaltic biorheological flow through an asymmetric microchannel: mathematical model. Meccanica **53**(8), 2079–2090 (2018)
6. Jhorar, R., Tripathi, D., Bhatti, M.M., Ellahi, R.: Electroosmosis modulated biomechanical transport through asymmetric microfluidics channel. Indian J. Phys., 1–10 (2018)
7. Ranjit, N.K., Shit, G.C., Tripathi, D.: Joule heating and zeta potential effects on peristaltic blood flow through porous micro vessels altered by electro-hydrodynamic. Microvasc. Res. **117**, 74–89 (2018)
8. Prakash, J., Tripathi, D.: Electroosmotic flow of Williamson ionic nanoliquids in a tapered microfluidic channel in presence of thermal radiation and peristalsis. J. Mol. Liq. **256**, 352–371 (2018)
9. Tripathi, D., Yadav, A., Bég, O.A., Kumar, R.: Study of microvascular non-Newtonian blood flow modulated by electroosmosis. Microvasc. Res. **117**, 28–36 (2018)
10. Das, S., Tarafdar, B., Jana, R.N., Makinde, O.D.: Influence of wall conductivities on a fully developed mixed-convection magnetohydrodynamic nanofluid flow in a vertical channel. J. Eng. Phys. Thermophys. **91**(3), 784–796 (2018)
11. Hassan, M.A., Godh, W.A., Moatimid, G.M., El-dabe, N.T.: Wall properties of peristaltic MHD nanofluid flow through porous channel. Int. J. Fluid Mech. Res. (2018)
12. Alghamdi, A.M., Gala, S., Ragusa, M.A.: New regularity criteria for the 3D Hall-MHD equations. In: Annales Polonici Mathematici. Instytut Matematyczny Polskiej Akademii Nauk., vol. 121, pp. 7–20 (2018)
13. Ahmed, N., Vieru, D., Fetecau, C., Shah, N.A.: Convective flows of generalized time-nonlocal nanofluids through a vertical rectangular channel. Phys. Fluids **30**(5), 052002 (2018)
14. Pramuanjaroenkij, A., Tongkratoke, A., Kakaç, S.: Numerical study of mixing thermal conductivity models for nanofluid heat transfer enhancement. J. Eng. Phys. Thermophys. **91**(1), 104–114 (2018)
15. Arabpour, A., Karimipour, A., Toghraie, D., Akbari, O.A.: Investigation into the effects of slip boundary condition on nanofluid flow in a double-layer microchannel. J. Therm. Anal. Calorim. **131**(3), 2975–2991 (2018)
16. Akbarzadeh, M., Rashidi, S., Karimi, N., Omar, N.: First and second laws of thermodynamics analysis of nanofluid flow inside a heat exchanger duct with wavy walls and a porous insert. J. Therm. Anal. Calorim., 1–18 (2018)
17. Mosayebidorcheh, S., Hatami, M.: Analytical investigation of peristaltic nanofluid flow and heat transfer in an asymmetric wavy wall channel (Part I: Straight channel). Int. J. Heat Mass Transf. **126**, 790–799 (2018)
18. Mosayebidorcheh, S., Hatami, M.: Analytical investigation of peristaltic nanofluid flow and heat transfer in an asymmetric wavy wall channel (Part II: Divergent channel). Int. J. Heat Mass Transf. **126**, 800–808 (2018)
19. Rahman, M.: Study on magnetohydrodynamic nanofluid flow through expanding or contracting channel with permeable walls (2018)
20. Prakash, J., Sharma, A., Tripathi, D.: Thermal radiation effects on electroosmosis modulated peristaltic transport of ionic nanoliquids in biomicrofluidics channel. J. Mol. Liq. **249**, 843–855 (2018)
21. Gala, S., Guo, Z., Ragusa, M.A.: A remark on the regularity criterion of Boussinesq equations with zero heat conductivity. Appl. Math. Lett. **27**, 70–73 (2014)
22. Gala, S., Ragusa, M.A., Sawano, Y., Tanaka, H.: Uniqueness criterion of weak solutions for the dissipative quasi-geostrophic equations in Orlicz–Morrey spaces. Appl. Anal. **93**(2), 356–368 (2014)
23. Noreen, S.: Peristaltically assisted nanofluid transport in an asymmetric channel. Karbala Int. J. Mod. Sci. **4**(1), 35–49 (2018)
24. Latha, R., Kumar, B.R., Makinde, O.D.: Effects of heat dissipation on the peristaltic flow of Jeffery and Newtonian fluid through an asymmetric channel with porous medium. In: Defect and Diffusion Forum, vol. 387, pp. 218–243. Trans Tech Publications, Scientific.Net (2018)
25. Latha, R., Kumar, B.R., Makinde, O.D.: Peristaltic flow of couple stress fluid in an asymmetric channel with partial slip. In: Defect and Diffusion Forum, vol. 387, pp. 385–402. Trans Tech Publications, Scientific.Net (2018)
26. Noreen, S.: Magneto-thermo hydrodynamic peristaltic flow of Eyring–Powell nanofluid in asymmetric channel. Nonlinear Eng. **7**(2), 83–90 (2018)
27. Abd Elmaboud, Y., Abdelsalam, S.I., Mekheimer, K.S.: Couple stress fluid flow in a rotating channel with peristalsis. J. Hydrodyn. **30**, 307–316 (2018)
28. Bhatti, M.M., Zeeshan, A., Tripathi, D., Ellahi, R.: Thermally developed peristaltic propulsion of magnetic solid particles in biorheological fluids. Indian J. Phys. **92**(4), 423–430 (2018)
29. Elmaboud, Y.A., Abdelsalam, S.I., Mekheimer, K.S., Vafai, K.: Electromagnetic flow for two-layer immiscible fluids. Int. J. Eng. Sci. Technol. (2018)
30. Saravana, R., Vajravelu, K., Sreenadh, S.: Influence of compliant walls and heat transfer on the peristaltic transport of a Rabinowitsch fluid in an inclined channel. Z. Naturforsch. A **73**(9), 833–843 (2018)